# How much helicity is needed to drive large-scale dynamos?

Simon Candelaresi[1,2] and Axel Brandenburg[1,2]

[1]NORDITA, KTH Royal Institute of Technology and Stockholm University, Roslagstullsbacken 23, SE-10691 Stockholm, Sweden
[2]Department of Astronomy, AlbaNova University Center, Stockholm University, SE-10691 Stockholm, Sweden

(Dated: August 23, 2012, Revision: 1.67 )

Magnetic field generation on scales large compared with the scale of the turbulent eddies is known to be possible via the so-called $\alpha$ effect when the turbulence is helical and if the domain is large enough for the $\alpha$ effect to dominate over turbulent diffusion. Using three-dimensional turbulence simulations, we show that the energy of the resulting mean magnetic field of the saturated state increases linearly with the product of normalized helicity and the ratio of domain scale to eddy scale, provided this product exceeds a critical value around unity. This implies that large-scale dynamo action commences when the normalized helicity is larger than the inverse scale ratio. Recent findings of a smaller minimal helicity may be due to the onset of small-scale dynamo action at large magnetic Reynolds numbers. The onset of large-scale dynamo action is difficult to establish when the kinetic helicity is small.

PACS numbers:



## I. INTRODUCTION

The origin of magnetic fields in astrophysical bodies like the Earth, the Sun and galaxies is studied in the field of dynamo theory. The temporal variation and strength of those fields rules out a primordial origin, through which the magnetic field would have been created in the early Universe. For magnetic fields with energies of the equipartition value, i.e. the turbulent kinetic energy of the medium, the primordial hypothesis explains their strength after creation, but falls short of explaining how the field outlives billions of years of resistive decay [1].

In dynamo theory, astrophysical plasmas are considered sufficiently well conducting fluids where the inertia of the charge-carrying particles can be neglected. In this approximation the equations of magnetohydrodynamics (MHD) provide an adequate model of the medium. In this framework it has been studied under which conditions magnetic fields of equipartition strength and scales larger than the turbulent motions are created and sustained [2].

A successful theoretical model describing the dynamo's behavior is the mean-field theory. It relates the small-scale turbulent motions to the mean magnetic field via the so-called $\alpha$ effect, which provides the energy input via helical turbulent forcing. During the kinematic phase, i.e. negligible back reaction of the magnetic field on the fluid, the $\alpha$ effect gives a positive feedback on the large-scale magnetic field, which results in its exponential growth. Already the consideration of the kinematic MHD equations with negligible Lorentz force sheds light on the growth rate of the different modes of the magnetic field during the kinematic phase. In the kinematic phase the growth rate $\lambda$ at wave number $k$ is given by [2]

$$\lambda = \alpha k - \eta_{\rm T} k^2 = (C_\alpha - 1)\eta_{\rm T} k^2, \tag{1}$$

where $C_\alpha = \alpha/\eta_{\rm T} k$ is the relevant dynamo number for the $\alpha^2$ dynamo, $\alpha$ is the $\alpha$ coefficient which is proportional to the small-scale kinetic helicity, and $\eta_{\rm T} = \eta + \eta_{\rm t}$ is the sum of molecular and turbulent magnetic diffusivity. Clearly, dynamo action occurs when $|C_\alpha| > C_\alpha^{\rm crit}$, where the onset condition is $C_\alpha^{\rm crit} = 1$. Standard estimates for isotropic turbulence in the high conductivity limit [2, 3] yield $\alpha = -(\tau/3)\langle \boldsymbol{\omega}\cdot\boldsymbol{u}\rangle$ and $\eta_{\rm t} = (\tau/3)\langle \boldsymbol{u}^2\rangle$, where $\tau$ is the correlation time of the turbulence, $\boldsymbol{\omega} = \boldsymbol{\nabla}\times\boldsymbol{u}$ is the vorticity and $\boldsymbol{u}$ is the velocity in the small-scale fields. Here $\langle . \rangle$ denote volume averages. Using $\eta_{\rm t} \gg \eta$, we have

$$C_\alpha = -\langle \boldsymbol{\omega}\cdot\boldsymbol{u}\rangle / k \langle \boldsymbol{u}^2\rangle. \tag{2}$$

It is convenient to define $\langle \boldsymbol{\omega}\cdot\boldsymbol{u}\rangle/k_{\rm f}\langle \boldsymbol{u}^2\rangle$ as the normalized kinetic helicity, $\epsilon_{\rm f}$, so $C_\alpha = -\epsilon_{\rm f} k_{\rm f}/k$. This scaling implies that the critical value of the normalized helicity $\epsilon_{\rm f}$ scales inversely proportional to the scale separation ratio, i.e. $\epsilon_{\rm f} \propto (k_{\rm f}/k)^{-1}$, where $k \ll k_{\rm f}$ is the wave number of the resulting large-scale magnetic field. This wave number can be equal to $k = k_1 \equiv 2\pi/L$, which is the smallest wave number in a periodic domain of size $L$.

In summary, the critical dynamo number $C_\alpha^{\rm crit}$, which decides between growing or decaying solutions of the large-scale dynamo (LSD), is proportional to the product of normalized helicity $\epsilon_{\rm f}$ and scale separation ratio $k_{\rm f}/k$. Therefore, the amount of helicity needed for the LSD is inversely proportional to the scale separation ratio, and not some higher power of it. It should be noted that the *normalized* kinetic helicity $\epsilon_{\rm f}$ used here is not the same as the *relative* kinetic helicity, $\tilde{\epsilon_{\rm f}} = \langle \boldsymbol{\omega}\cdot\boldsymbol{u}\rangle/(\omega_{\rm rms} u_{\rm rms})$. The two are related to each other via the relation

$$\tilde{\epsilon_{\rm f}}/\epsilon_{\rm f} = k_\omega/k_{\rm f}, \tag{3}$$

where $k_\omega \approx \omega_{\rm rms}/u_{\rm rms}$ is inversely proportional to the Taylor microscale. Here, the subscripts rms refer to root-mean-square values. For small Reynolds numbers, $k_\omega$ provides a useful estimate of the wave number $k_{\rm f}$ of the energy-carrying eddies. In contrast, for large Reynolds numbers Re, we expect $k_\omega/k_{\rm f}$ to be proportional to $\mathrm{Re}^{1/2}$, so $\tilde{\epsilon_{\rm f}}$ decreases correspondingly while $\epsilon_{\rm f}$ remains unchanged. Below we shall present new results suggesting that in the present case of helical turbulence the exponent is not 1/2 but 1/4.

To understand the saturation of a helical dynamo, it is important to understand the relation between the resulting large-scale field and the associated small-scale field. Indeed, the

growth of the large-scale field is always accompanied by a growth of small-scale magnetic field. Small-scale here means the scale of the underlying turbulent motions, which drive the dynamo. Conservation of total magnetic helicity causes a build up of magnetic helicity at large scales and of opposite sign at small scales [4, 5]. As the dynamo saturates, the largest scales of the magnetic field become even larger, which finally leads to a field of a scale that is similar to that of the system itself. This can be understood as being the result of an inverse cascade, which was first predicted based on closure calculations [6].

If the domain is closed or periodic, the build up of small-scale magnetic helicity causes the $\alpha$ effect to diminish, which marks the end of the exponential growth and could occur well before final saturation is reached. The dynamo then is said to be catastrophically quenched and, in a closed or periodic system, the subsequent growth to the final state happens not on a dynamical timescale, but on a resistive one. Quenching becomes stronger as the magnetic Reynolds number increases, which, for astrophysically relevant problems, means a total loss of the LSD within the timescales of interest. In the case of open boundaries magnetic helicity fluxes can occur, which can alleviate the quenching and allow for fast saturation of the large-scale magnetic field [7–10].

In a recent publication [11] it was argued that for periodic boundaries the critical value of $\epsilon_{\rm f}$ for LSD action to occur decreases with the scale separation ratio like $\epsilon_{\rm f}^{\rm crit} \propto (k_{\rm f}/k_1)^{-3}$. Their finding, however, is at variance with the predictions made using equation (1), which would rather suggest a dependence of $\epsilon_{\rm f}^{\rm crit} \propto (k_{\rm f}/k_1)^{-1}$ with $C_\alpha^{\rm crit} = 1$. This discrepancy could be a consequence of the criterion used in [11] for determining $C_\alpha^{\rm crit}$. The authors looked at the growth rate of the magnetic field after the end of the kinematic growth phase, but only at a small fraction of the resistive time. Therefore their results might well be contaminated by magnetic fields resulting from the small-scale dynamo (SSD). Earlier simulations [12] have demonstrated that for ${\rm Re_M} \geq 100$, the growth rate of the helical LSD approaches the well-known scaling of the non-helical SSD with $\lambda \propto {\rm Re}^{1/2}$, which corresponds to the turnover rate of the smallest turbulent eddies [13, 14].

Given that the LSD is best seen in the nonlinear regime [15], we decided to determine $C_\alpha^{\rm crit}$ from a bifurcation diagram by extrapolating to zero. In a bifurcation diagram we plot the energy of the mean or large-scale field versus $C_\alpha$. Simple considerations using the magnetic helicity equation applied to a homogeneous system in the steady state show that the current helicity must vanish [15]. In a helically driven system, this implies that the current helicity of the large-scale field must then be equal to minus the current helicity of the small-scale field. For a helical magnetic field this yields the value of $\langle\overline{\boldsymbol{B}}^2\rangle/B_{\rm eq}^2$ approximately as $\epsilon_{\rm f} k_{\rm f}/k_1$, i.e., proportional to $C_\alpha$. Here $B_{\rm eq} = (\mu_0\overline{\rho})^{1/2} u_{\rm rms}$ is the equipartition value of the magnetic field with the permeability $\mu_0$ and the mean density $\overline{\rho}$. Again, this suggests that the LSD is excited for $\epsilon_{\rm f} > (k_{\rm f}/k_1)^{-1}$ rather than some higher power of $k_{\rm f}/k_1$. This is a basic prediction that has been obtained from nonlinear mean-field dynamo models that incorporate magnetic helicity evolution [16] as well as from direct numerical simulations in the presence of shear [17]. The purpose of the present paper is to reinvestigate these results over a broader parameter range in the light of recent conflicting findings [11].

## II. THE MODEL

### A. Basic equations

The underlying equations for non-relativistic MHD, which we solve numerically, are given as

$$\frac{\partial}{\partial t}\boldsymbol{A} = \boldsymbol{U}\times\boldsymbol{B} - \eta\mu_0\boldsymbol{J}, \tag{4}$$

$$\frac{\rm D}{{\rm D}t}\boldsymbol{U} = -c_{\rm s}^2\boldsymbol{\nabla}\ln\rho + \frac{1}{\rho}\boldsymbol{J}\times\boldsymbol{B} + \boldsymbol{F}_{\rm visc} + \boldsymbol{f}, \tag{5}$$

$$\frac{\rm D}{{\rm D}t}\ln\rho = -\boldsymbol{\nabla}\cdot\boldsymbol{U}, \tag{6}$$

where $\boldsymbol{A}$ is the magnetic vector potential, $\boldsymbol{U}$ the velocity, $\boldsymbol{B}$ the magnetic field, $\eta$ the molecular magnetic diffusivity, $\mu_0$ the vacuum permeability, $\boldsymbol{J}$ the electric current density, $c_{\rm s}$ the isothermal sound speed, $\rho$ the density, $\boldsymbol{F}_{\rm visc}$ the viscous force, $\boldsymbol{f}$ the helical forcing term and ${\rm D}/{\rm D}t = \partial/\partial t + \boldsymbol{U}\cdot\boldsymbol{\nabla}$ the advective time derivative. The viscous force is given as $\boldsymbol{F}_{\rm visc} = \rho^{-1}\boldsymbol{\nabla}\cdot 2\nu\rho\mathsf{S}$, with the traceless rate of strain tensor $\mathsf{S}$ with components $\mathsf{S}_{ij} = \frac{1}{2}(u_{i,j}+u_{j,i}) - \frac{1}{3}\delta_{ij}\boldsymbol{\nabla}\cdot\boldsymbol{U}$ and the kinematic viscosity $\nu$. Commas denote partial derivatives.

The energy supply for a helically driven dynamo is provided by the forcing function $\boldsymbol{f} = \boldsymbol{f}(\boldsymbol{x},t)$, which is a helical function that is random in time. It is defined as

$$\boldsymbol{f}(\boldsymbol{x},t) = {\rm Re}\{N\boldsymbol{f}_{\boldsymbol{k}(t)}\exp[{\rm i}\boldsymbol{k}(t)\cdot\boldsymbol{x} + {\rm i}\phi(t)]\}, \tag{7}$$

where $\boldsymbol{x}$ is the position vector. The wave vector $\boldsymbol{k}(t)$ and the random phase $-\pi < \phi(t) \leq \pi$ change at every time step, so $\boldsymbol{f}(\boldsymbol{x},t)$ is $\delta$-correlated in time. For the time-integrated forcing function to be independent of the length of the time step $\delta t$, the normalization factor $N$ has to be proportional to $\delta t^{-1/2}$. On dimensional grounds it is chosen to be $N = f_0 c_{\rm s}(|\boldsymbol{k}|c_{\rm s}/\delta t)^{1/2}$, where $f_0$ is a non-dimensional forcing amplitude. We choose $f_0 = 0.02$ which results in a maximum Mach number of about 0.3 and an rms value of about 0.085. At each timestep we select randomly one of many possible wave vectors in a certain range around a given forcing wave number. The average wave number is referred to as $k_{\rm f}$. Transverse helical waves are produced via [14]

$$\boldsymbol{f}_{\boldsymbol{k}} = \mathsf{R}\cdot\boldsymbol{f}_{\boldsymbol{k}}^{\rm (nohel)} \quad \text{with} \quad \mathsf{R}_{ij} = \frac{\delta_{ij} - {\rm i}\sigma\epsilon_{ijk}\hat{k}_k}{\sqrt{1+\sigma^2}}, \tag{8}$$

where $\sigma$ is a measure of the helicity of the forcing and $\sigma = 1$ for positive maximum helicity of the forcing function. Furthermore,

$$\boldsymbol{f}_{\boldsymbol{k}}^{\rm (nohel)} = (\boldsymbol{k}\times\boldsymbol{e})\,/\sqrt{\boldsymbol{k}^2 - (\boldsymbol{k}\cdot\boldsymbol{e})^2} \tag{9}$$

is a non-helical forcing function, where $\boldsymbol{e}$ is an arbitrary unit vector not aligned with $\boldsymbol{k}$; note that $|\boldsymbol{f}_{\boldsymbol{k}}|^2 = 1$ and

$$\boldsymbol{f}_{\boldsymbol{k}}\cdot({\rm i}\boldsymbol{k}\times\boldsymbol{f}_{\boldsymbol{k}})^* = 2\sigma k/(1+\sigma^2), \tag{10}$$

so the relative helicity of the forcing function in real space is $2\sigma/(1+\sigma^2)$.

For comparison with earlier work, we shall also use in one case an ABC-flow forcing function,

$$\boldsymbol{f}(\boldsymbol{x}) = \frac{f_0}{\sqrt{\frac{3}{2}(1+\sigma^2)}} \begin{pmatrix} \sin X_3 + \sigma \cos X_2 \\ \sin X_1 + \sigma \cos X_3 \\ \sin X_2 + \sigma \cos X_1 \end{pmatrix}, \qquad (11)$$

where $X_i = k_{\rm f} x_i + \theta_i$ and $\theta_i = \theta_0 \cos \omega_i t$ are time-dependent phases that vary sinusoidally with frequencies $\omega_i$ and amplitude $\theta_0$. This forcing function is easy to implement and serves therefore as a proxy of helical turbulence; see Ref. [11, 18], where the phases changed randomly. We have restricted ourselves to the special case where the coefficients in front of the trigonometric functions are unity, but those could be made time-dependent too; see Ref. [19]. However, as we will see below, ABC-flow driven dynamos do not show some crucial aspects of random plane wave-forced helical turbulence. Most of the results presented below concern the forcing function (7) and only one case with Eq. (11) will be considered at the end.

Our model is governed by several non-dimensional parameters. In addition to the scale separation ratio $k_{\rm f}/k_1$, introduced above, there are the magnetic Reynolds and Prandtl numbers

$$\mathrm{Re_M} = u_{\rm rms}/\eta k_{\rm f}, \quad \mathrm{Pr_M} = \nu/\eta. \qquad (12)$$

These two numbers also define the fluid Reynolds number, $\mathrm{Re} = u_{\rm rms}/\nu k_{\rm f} = \mathrm{Re_M}/\mathrm{Pr_M}$. The maximum values that can be attained are limited by the numerical resolution and become more restrictive at larger scale separation. The calculations have been performed using the PENCIL CODE (see http://pencil-code.googlecode.com) at resolutions of up to $512^3$ mesh points.

### B. Mean-field interpretation

The induced small-scale motions $\boldsymbol{u}$ are helical and give rise to the kinetic $\alpha$ effect [3]

$$\alpha_{\rm K} = -\frac{\langle \boldsymbol{\omega} \cdot \boldsymbol{u} \rangle}{3 u_{\rm rms} k_{\rm f}}. \qquad (13)$$

The relevant $\alpha$ effect for dynamo action is the sum of the kinetic and magnetic $\alpha$ [20]:

$$\alpha = \frac{-\langle \boldsymbol{\omega} \cdot \boldsymbol{u} \rangle + \langle \boldsymbol{j} \cdot \boldsymbol{b} \rangle / \langle \rho \rangle}{3 u_{\rm rms} k_{\rm f}}. \qquad (14)$$

The resulting large-scale fields are partially helical, which means one can write

$$\langle \boldsymbol{J} \cdot \boldsymbol{B} \rangle = \epsilon_{\rm m} k_{\rm m} \langle \boldsymbol{B}^2 \rangle, \qquad (15)$$

with large-scale wave vector $k_{\rm m}$ and corresponding fractional helicity $\epsilon_{\rm m}$. However, in the cases considered below the domain is triply periodic, so the solutions are Beltrami fields for which $k_{\rm m} = k_1$ and $\epsilon_{\rm m} = 1$ is an excellent approximation, and only $\epsilon_{\rm f}$ will take values less unity. Nevertheless, in some expressions we retain the $\epsilon_{\rm m}$ factor for clarity. For example, the saturation value of the large-scale magnetic field, $B_{\rm sat}$, is given by [16]

$$B_{\rm sat}^2/B_{\rm eq}^2 = (|C_\alpha|/\epsilon_{\rm m} - 1)\, \iota, \qquad (16)$$

where $C_\alpha = \alpha_{\rm K}/(\eta_{\rm T} k_1)$ is the relevant dynamo number based on the smallest wavenumber in the domain and $\iota = 1 + 3/\mathrm{Re_M} \equiv \eta_{\rm T}/\eta_{\rm t}$ is a correction factor resulting from the fact that $\eta_{\rm T}$ is slightly bigger than $\eta_{\rm t}$. The factor 3 in the expression for $\iota$ results from our definition of $\mathrm{Re_M}$ and the fact that [21]

$$\eta_{\rm t} = u_{\rm rms}/3k_{\rm f} = \eta \mathrm{Re_M}/3. \qquad (17)$$

Equation (16) shows clearly the onset condition $|C_\alpha| > |\epsilon_{\rm m}| \approx 1$. Using Eqs. (13) and (17), we find

$$C_\alpha = -\frac{\langle \boldsymbol{\omega} \cdot \boldsymbol{u} \rangle}{\iota k_1 u_{\rm rms}^2} = -\frac{\epsilon_{\rm f} k_{\rm f}}{\iota k_1}. \qquad (18)$$

From equation (16) we can derive the critical value of the normalized helicity $\epsilon_{\rm f}$ as a function of the scale separation ratio. Setting $C_\alpha$ to is critical value ($|C_\alpha| = \epsilon_{\rm m}$) we obtain

$$\epsilon_{\rm f}^{\rm crit} = \iota \epsilon_{\rm m} \left( \frac{k_{\rm f}}{k_1} \right)^{-1}, \qquad (19)$$

which is at variance with the findings in [11].

Once the dynamo is excited and has reached a steady state, not only $\alpha$ but also $\eta_{\rm t}$ will be suppressed. This can be taken into account using a quenching factor $g(\overline{B})$, so $\eta_{\rm t}(\overline{B}) = \eta_{\rm t0} g(\overline{B})$ with $g = (1 + \tilde{g}|\overline{\boldsymbol{B}}|/B_{\rm eq})^{-1}$. Equation (16) is then modified and reads $B_{\rm sat}^2/B_{\rm eq}^2 = (|C_\alpha| - C_{\alpha 0})\iota/\epsilon_{\rm m}$ with

$$C_{\alpha 0} = [1 - (1-g)/\iota]\epsilon_{\rm m}. \qquad (20)$$

Note that $C_{\alpha 0} = \epsilon_{\rm m}^{-1}$ in the unquenched case, i.e., for $g = 1$.

### C. Simulation strategy

We recall that our forcing term $\boldsymbol{f}$ in equation (7) is a stochastic forcing centered around the wave number $k_{\rm f}$. In contrast to [11] this forcing is delta-correlated in time. The fractional helicity of the helical forcing is a free parameter. The simulation domain is a periodic cube with dimensions $2\pi$. Due to the cubic geometry of the domain the large-scale magnetic field can orient itself in 3 possible directions. Therefore we compute three possible planar averages ($xy$, $xz$, and $yz$ averages). From their resistive evolution we infer their saturation values at the end of the resistive phase. The strongest field gives then the relevant mean-field $\overline{\boldsymbol{B}}$.

Since $\overline{\boldsymbol{B}}$ is helical and magnetic helicity can only change on resistive timescales, the temporal evolution of the energy of the mean magnetic field, $M(t)$, is given by [15]

$$M(t) = M_0 - M_1 e^{-t/\tau}, \qquad (21)$$

where $\tau^{-1} = 2\eta \epsilon_{\rm m}^2 k_1^2$ is known, $M_0 = B_{\rm sat}^2$ is the square of the desired saturation field strength, and $M_1$ is an unknown constant that can be positive or negative, depending

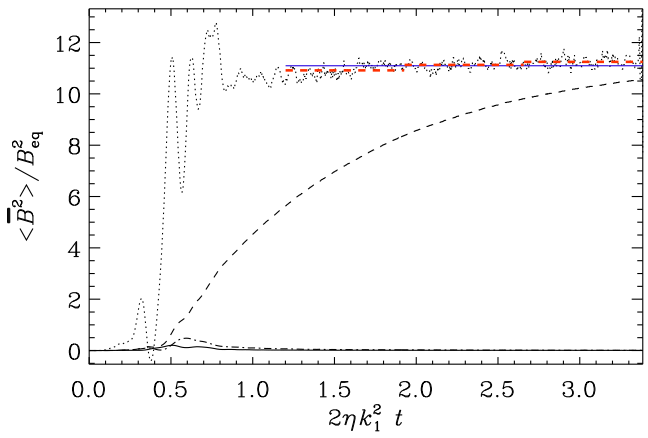


FIG. 1: Example showing the evolution of the normalized $\langle\overline{\boldsymbol{B}}^2\rangle$ (dashed) and that of $\langle\overline{\boldsymbol{B}}^2\rangle+\tau{\rm d}\langle\overline{\boldsymbol{B}}^2\rangle/{\rm d}t$ (dotted), compared with its average in the interval $1.2\leq 2\eta k_1^2 t\leq 3.5$ (horizontal blue solid line), as well as averages over 3 subintervals (horizontal red dashed lines). Here, $\overline{\boldsymbol{B}}$ is evaluated as an $xz$ average, $\langle\boldsymbol{B}\rangle_{xz}$. For comparison we also show the other two averages, $\langle\boldsymbol{B}\rangle_{xy}$ (solid) and $\langle\boldsymbol{B}\rangle_{xy}$ (dash-dotted), but their values are very small.

on whether the initial magnetic field of a given calculation was smaller or larger than the final value. (Here, an initial field could refer to the last snapshot of another calculation with similar parameters, for example.) The functional behavior given by Eq. (21) allows us to determine $B_{\rm sat}^2$ as the time average of $M+\tau{\rm d}M/{\rm d}t$, which should only fluctuate about a constant value, i.e.,

$$B_{\rm sat}^2\approx\frac{1}{t_2-t_1}\int_{t_1}^{t_2}\left[\langle\overline{\boldsymbol{B}}^2\rangle(t')+\tau\frac{\rm d}{{\rm d}t'}\langle\overline{\boldsymbol{B}}^2\rangle\right]{\rm d}t'. \quad (22)$$

This technique has the advantage that we do not need to wait until the field reaches its final saturation field strength. Error bars can be estimated by computing this average for each third of the full time series and taking the largest departure from the average over the full time series. An example is shown in Fig. 1, where we see $\langle\overline{\boldsymbol{B}}^2\rangle$ still growing while $\langle\overline{\boldsymbol{B}}^2\rangle+\tau{\rm d}\langle\overline{\boldsymbol{B}}^2\rangle/{\rm d}t$ is nearly constant when $\langle\overline{\boldsymbol{B}}^2\rangle$ has reached a value less than half its final one.

## III. RESULTS

### A. Dependence of kinetic helicity on $\sigma$

We recall that the relative helicity of the forcing function is $\boldsymbol{f}\cdot\boldsymbol{\nabla}\times\boldsymbol{f}/[\boldsymbol{f}_{\rm rms}(\boldsymbol{\nabla}\times\boldsymbol{f})_{\rm rms}]=2\sigma/(1+\sigma^2)$. This imposes then a similar variation onto the relative kinetic helicity, $\tilde{\epsilon_{\rm f}}=\langle\boldsymbol{\omega}\cdot\boldsymbol{u}\rangle/\omega_{\rm rms}u_{\rm rms}$; see Fig. 2(a). However, as discussed above, $\tilde{\epsilon_{\rm f}}$ is smaller than $\epsilon_{\rm f}$ by a factor $k_\omega/k_{\rm f}$, which depends on the Reynolds number. It turns out that $\epsilon_{\rm f}$ matches almost exactly the values of $2\sigma/(1+\sigma^2)$; see Fig. 2(b).

The theoretically expected scaling $k_\omega/k_{\rm f}\propto{\rm Re}^{1/2}$ is a well-known result for non-helical turbulence [22], but for

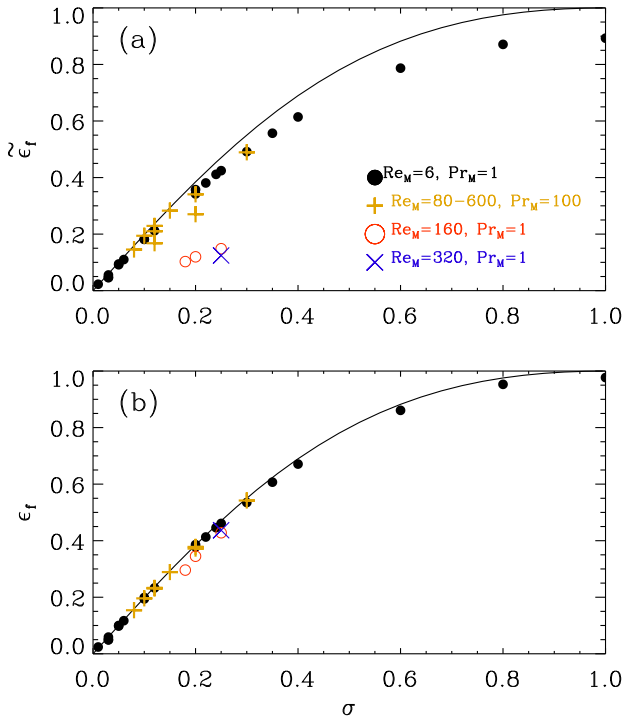


FIG. 2: Dependence of relative kinetic helicity $\tilde{\epsilon_{\rm f}}$ (a) and normalized kinetic helicity $\epsilon_{\rm f}$ (b) on the helicity parameter $\sigma$ of the forcing function Eq. (8) together with the analytical expression $2\sigma/(1+\sigma^2)$ (solid line).

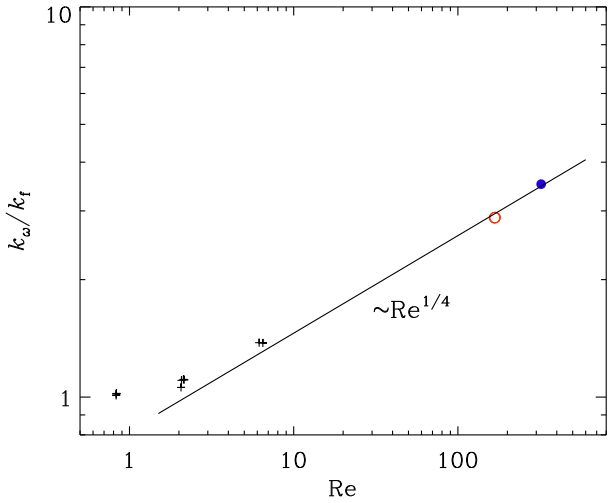


FIG. 3: Dependence of $k_\omega/k_{\rm f}$ on Re. The open and closed circles correspond to runs with ${\rm Pr_M}=1$, while the $+$ signs correspond to runs with ${\rm Pr_M}=100$, so ${\rm Re}={\rm Re_M}/{\rm Pr_M}$.

helical turbulence those scaling relations are modified; see, e.g., Ref. [23]. For our current data we find that $k_\omega/k_{\rm f}\approx 0.8\,{\rm Re}^{1/4}$; see Fig. 3. The reason for this power law behavior is however unclear.

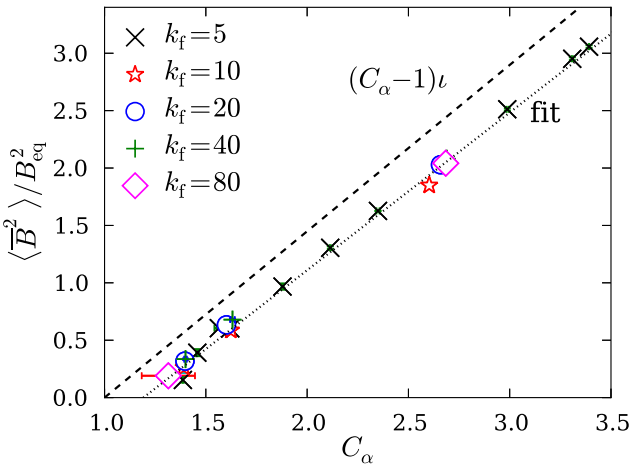


FIG. 4: Steady state values of $\langle\overline{\boldsymbol{B}}^2\rangle/B_{\rm eq}^2$ as a function of $C_\alpha$ together with the theoretical prediction from equation (16) (dashed line) and a linear fit (dotted line).

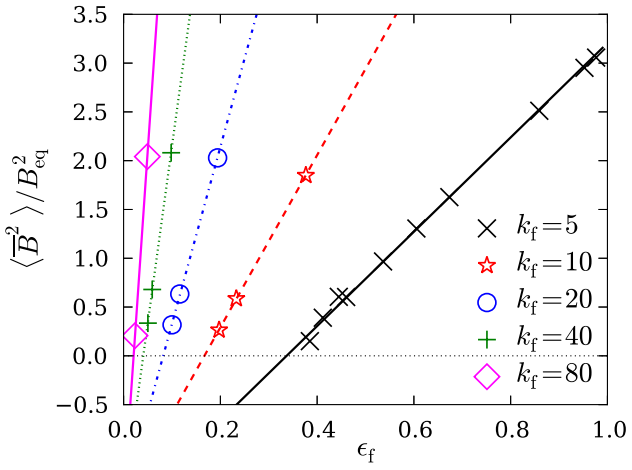


FIG. 5: Steady state values of $\langle\overline{\boldsymbol{B}}^2\rangle/B_{\rm eq}^2$ as a function of $\epsilon_{\rm f}$ for various scale separation values $k_{\rm f}/k_1$ together with linear fits.

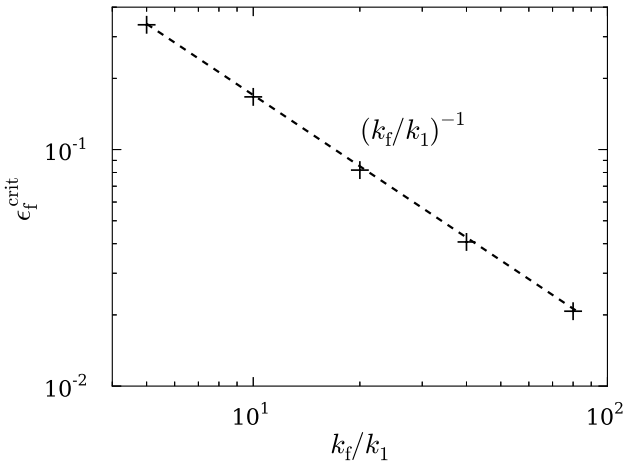


FIG. 6: Critical value for the normalized kinetic helicity $\epsilon_{\rm f}$ for which LSD action occurs for different scale separations.

### B. Dependence on scale separation

We perform simulations with different forcing wave numbers $k_{\rm f}$ and different values of $\epsilon_{\rm f}$ at approximately constant magnetic Reynolds number, $\mathrm{Re_M}\approx 6$, and fixed magnetic Prandtl number, $\mathrm{Pr_M}=1$. Near the end of the resistive saturation phase we look at the energy of the strongest mode at $k=k_1$, using the method described in § II C.

As seen from Eq. (16), mean-field considerations predict a linear increase of the saturation magnetic energy with $C_\alpha$ and onset at $C_\alpha=1$. This behavior is reproduced in our simulation (Fig. 4), where we compare the theoretical prediction with the simulation results. For different values of $k_{\rm f}/k_1$ and $C_\alpha$ we extrapolate the critical value $C_\alpha^{\rm crit}\approx 1.2$ (Fig. 4), which gives the critical values $\epsilon_{\rm f}^{\rm crit}\approx 1.2\iota\,(k_{\rm f}/k_1)^{-1}=1.7\,(k_{\rm f}/k_1)^{-1}$ for which the LSD is excited. For each scale separation value we plot the dependence of $\langle\overline{\boldsymbol{B}}^2\rangle/B_{\rm eq}^2$ on $\epsilon_{\rm f}$ (Fig. 5) and make linear fits. From these fits we can extrapolate the critical values $\epsilon_{\rm f}^{\rm crit}$, for which the LSD gets excited (Fig. 6), which gives again $\epsilon_{\rm f}^{\rm crit}\approx 1.7\,(k_{\rm f}/k_1)^{-1}$.

It is noteworthy that the graph of $\langle\overline{\boldsymbol{B}}^2\rangle/B_{\rm eq}^2$ versus $C_\alpha$ deviates systematically (although only by a small amount) from the theoretically expected value, $(C_\alpha-1)\iota$. While the slope is rather close to the expected one, the onset of LSD is slightly delayed and occurs at $C_\alpha\approx 1.2$ instead of 1. The reason for this is not clear, although one might speculate that it could be modelled by adopting modified effective values of $\iota$ or $\epsilon_{\rm m}$ in Eq. (20). Apart from such minor discrepancies with respect to the simple theory, the agreement is quite remarkable. Nevertheless, we must ask ourselves whether this agreement persists for larger values of the magnetic Reynolds number. This will be addressed in § III C.

At this point we should note that there is also a theoretical prediction for the energy in the magnetic fluctuations, namely $\langle\boldsymbol{b}^2\rangle/B_{\rm eq}^2\approx(C_\alpha-C_\alpha^{\rm crit})/C_\alpha$. Nonetheless, the results shown in Fig. 7 deviate from this relation and are better described by a modified formula

$$\langle\boldsymbol{b}^2\rangle/B_{\rm eq}^2\propto 1-(C_\alpha^{\rm crit}/C_\alpha)^n\quad(\text{with } n\approx 4).\qquad(23)$$

Again, the reason for this departure is currently unclear.

### C. Dependence on $\mathrm{Re_M}$

To examine whether there is any unexpected dependence of the onset and the energy of the mean magnetic field on $\mathrm{Re_M}$ and to approach the parameters used in [11], who used values up to $\mathrm{Re_M}=1500$, we now consider larger values of the magnetic Reynolds number. This widens the inertial range significantly and leads to the excitation of the SSD. Higher values of

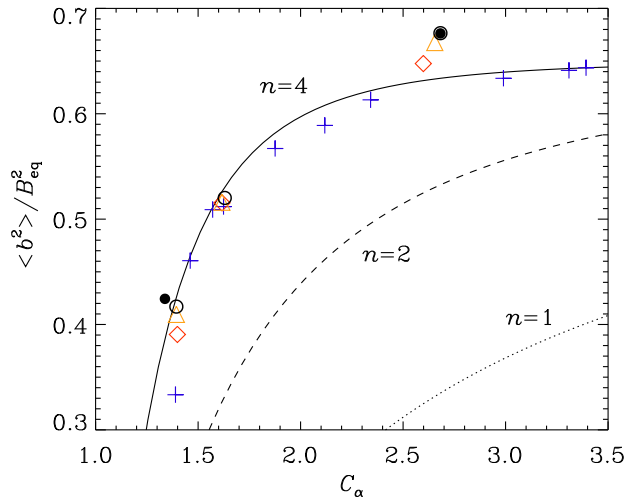


FIG. 7: Steady state values of $\langle \boldsymbol{b}^2 \rangle / B_{\rm eq}^2$ as a function of $C_\alpha$ together with the fit formula from equation (23) with $n = 4$, compared with $n = 1$ (dotted) and $n = 2$ (dashed).

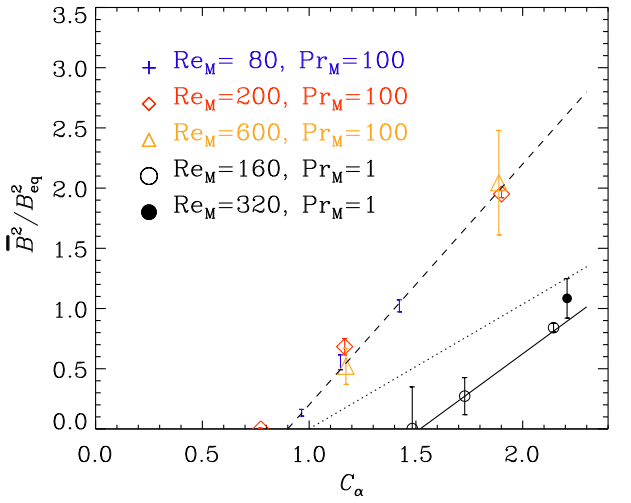


FIG. 8: Steady state values of $\langle \overline{\boldsymbol{B}}^2 \rangle / B_{\rm eq}^2$ as a function of $C_\alpha$ for $\mathrm{Pr_M} = 100$ (dashed line) and $\mathrm{Pr_M} = 1$ (solid line) for $k_{\rm f}/k_1 = 5$ and different values of $\mathrm{Re_M}$ (different symbols), compared with the theoretical prediction (dotted line).

$\mathrm{Re_M}$ can more easily be reached at larger values of $\mathrm{Pr_M}$. This is because at large values of $\mathrm{Pr_M}$, most of the injected energy is dissipated viscously rather than resistively, leaving less energy to be channelled down the magnetic cascade [24]. This is similar to the case of *small* values of $\mathrm{Pr_M}$, where larger *fluid* Reynolds numbers can be reached because then most of the energy is dissipated resistively [12]. Here, however, we shall be concerned with the former case of large values of $\mathrm{Pr_M}$.

The results for $\mathrm{Pr_M} = 100$ are presented in Fig. 8 for different values of $\epsilon_{\rm f}$ and $\mathrm{Re_M}$ being either 80, 200, or 600. Most importantly, it turns out that the critical value for the onset of LSD is not much changed. We now find $C_\alpha^{\rm crit} \approx 0.9$ instead

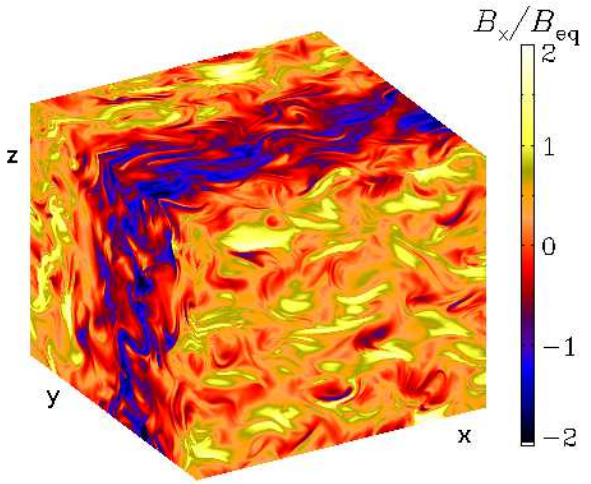


FIG. 9: Visualization of $B_x$ on the periphery of the domain for $\mathrm{Pr_M} = 100$ after resistive saturation.

of 1. Furthermore, the dependence of $\langle \overline{\boldsymbol{B}}^2 \rangle / B_{\rm eq}^2$ on $C_\alpha$, and thus also the value of $C_\alpha^{\rm crit}$, are the same for all three values of $\mathrm{Re_M}$. It is however surprising that it is now even below unity. Furthermore, the slope is different from that of Fig. 4: it is now closer to 2 than to the earlier value of 1. This discrepancy with the theory can be easily explained by arguing that the relevant value of $B_{\rm eq}$ has been underestimated in the low $\mathrm{Pr_M}$ cases. Looking at the power spectrum of the high $\mathrm{Pr_M}$ simulations in Fig. 10(a), we see that the kinetic energy is indeed subdominant and does not provide a good estimate of the magnetic energy of the small-scale field $\langle \boldsymbol{b}^2 \rangle / 2\mu_0$. By contrast, for $\mathrm{Pr_M} = 1$, the magnetic and kinetic energy spectra are similar at all scales except near $k = k_1$; see Fig. 10(b). The slight super-equipartition for $k > k_{\rm f}$ is also typical of small-scale dynamos [14].

A visualization of the magnetic field in this case is given in Fig. 9, where we show $B_x$ on the periphery of the computational domain. The magnetic field has now clearly strong gradients locally, while still being otherwise dominated by a large-scale component at $k = k_1$. In this case the large-scale field shows variations only in the $y$ direction and is of the form

$$\overline{\boldsymbol{B}} = (\sin k_1 y, 0, \cos k_1 y)\, B_{\rm sat}. \tag{24}$$

This field has negative magnetic helicity, so $\overline{\boldsymbol{J}} \cdot \overline{\boldsymbol{B}} = -k_1 \overline{\boldsymbol{B}}^2$, as expected for a forcing function with negative helicity.

We have argued that the reason for the larger slope in the graph of $\langle \overline{\boldsymbol{B}}^2 \rangle$ versus $C_\alpha$ is related to $B_{\rm eq}$ being underestimated for large values of $\mathrm{Pr_M}$. To confirm this, we now consider calculations with $\mathrm{Pr_M} = 1$, two different values of $\epsilon_{\rm f}$, and fixed values of $\mathrm{Re_M}$ (either 160 or 320), and fixed scale separation ratio $k_{\rm f}/k_1 = 5$. We see in Fig. 8 that the slope is indeed smaller. Furthermore, $C_\alpha^{\rm crit}$ is now above 1, and even larger than at low $\mathrm{Re_M}$ (now $C_\alpha^{\rm crit} \approx 1.5$ instead of 1.2).

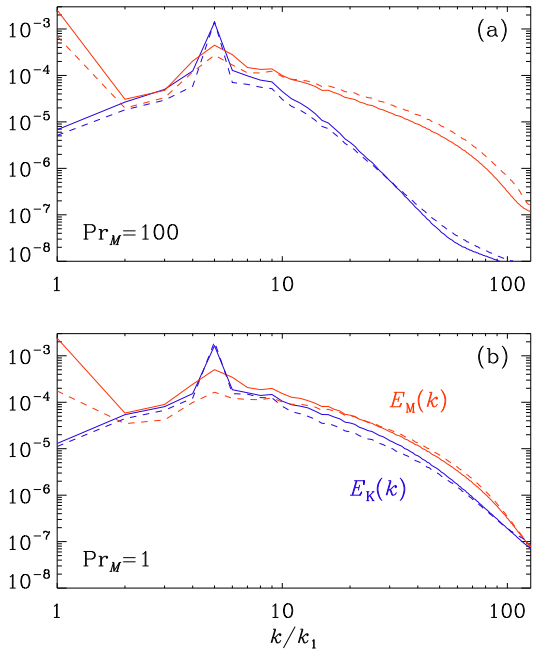


FIG. 10: Comparison of kinetic and magnetic energy spectra for $\mathrm{Pr_M} = 100$ (upper panel) and $\mathrm{Pr_M} = 1$ (lower panel) for $\sigma = 0.2$ (solid lines) and 0.12 (dashed lines).

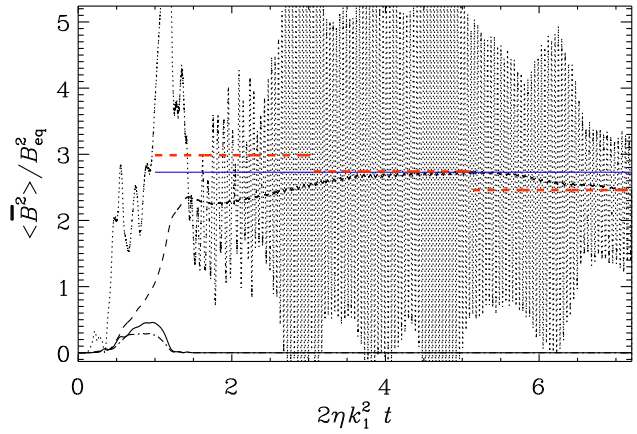


FIG. 11: Similar to Fig. 1, but for time-dependent ABC-flow driving. As in Fig. 1, we have here $k_\mathrm{f}/k_1 = 15$ and $\mathrm{Re_M} \approx 4$.

### D. ABC-flow forcing

In this paper we have used the fact that the saturation field strength is described by Eq. (16). While this is indeed well obeyed for our randomly driven flows, this does not seem to be the case for turbulence driven by ABC-flow forcing. We demonstrate this by considering a case that is similar to that shown in Fig. 1, where $\mathrm{Re_M} \approx 6$ in the saturated state. We thus use Eq. (11) with $\sigma = \theta_0 = 1$ and $k_\mathrm{f}/k_1 = 15$. The *kinematic* flow velocity reaches an equilibrium rms velocity of $U_0 = f_0/\nu k_\mathrm{f}^2$. The magnetic Reynolds number based on this velocity is $U_0/\eta k_\mathrm{f}$, which is chosen to be 13, so that during *saturation* the resulting value of $\mathrm{Re_M}$ is about 6, just as in Fig. 1. For the $x$, $y$, and $z$ components we take different forcing frequencies such that $\omega_i/k_1 U_0$ is 10, 11, and 9 for $i = 1$, 2, and 3, respectively. These values correspond approximately to the inverse correlation times used in [11]. The result is shown in Fig. 11. It turns out that the magnetic field grows initially as expected, based on Eq. (21), but then the final saturation phase is cut short below $B_{\rm sat}^2/B_{\rm eq}^2 \approx 3$ rather than the value 12 found with random wave forcing. This is reminiscent of inhomogeneous dynamos in which magnetic helicity fluxes operate. In homogeneous systems, however, magnetic helicity flux divergences have only been seen if there is also shear [25]. In any case, the present behavior is unexpected and suggests that the effective value of $C_\alpha$ is reduced. Using the test-field method [26, 27], we have confirmed that the actual value of $C_\alpha$ is not reduced. The dynamo is therefore excited, but the value implied for the effective helicity is reduced.

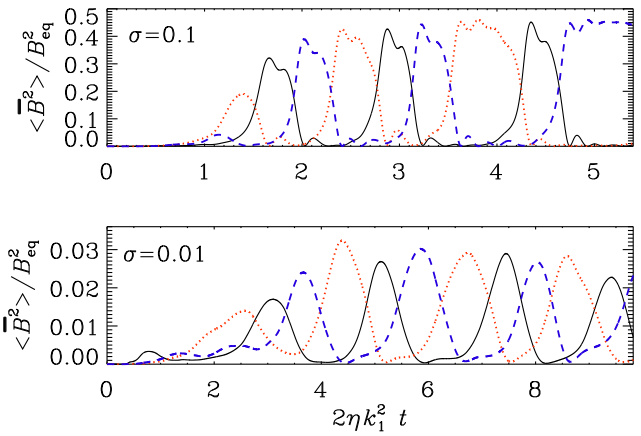


FIG. 12: Dependence of the normalized $\langle \overline{\boldsymbol{B}}^2 \rangle$ for different planar averages: $yz$ (black), $xz$ (red, dotted), and $xy$ (blue, dashed), for $\sigma = 0.1$ (upper panel) and $\sigma = 0.01$ (lower panel).

Another possibility is that, especially for small values of $\sigma$, the ABC-flow has non-generic dynamo properties that emulate aspects of large-scale dynamos. An example is shown in Fig. 12 where we plot the time evolution of all three planar averages ($yz$, $xz$, and $xy$). Even for $\sigma = 0.01$, large-scale magnetic fields are still excited, but the field orientation changes periodically on a timescale of 1–2 diffusion times. This is obviously a fascinating topic for further research, but it is unrelated to our main question regarding the minimal helicity of generic turbulent dynamos. The main point of this section is to emphasize the limited usefulness of ABC-flow dynamos. Another such example are dynamos driven by the Galloway-Proctor flow, which also has a number of peculiar features; see Ref. [28].

## IV. CONCLUSIONS

In this paper we have studied the simplest possible LSD and have investigated the dependence of its saturation amplitude on the amount of kinetic helicity in the system. We recall that the case of a periodic domain has already been investigated in some detail [29, 30], and that theoretical predictions in the case with shear [16] have been verified numerically for fractional helicities [17]. Yet the issue has now attracted new interest in view of recent results suggesting that, in the limit of large scale separation, the amount of kinetic helicity needed to drive the LSD might actually be much smaller than what earlier calculations have suggested. This was surprising given the earlier confirmations of the theory. As explained above, the reason for the conflicting earlier results may be the fact that the LSD cannot be safely isolated in the linear regime, because it will be dominated by the SSD or, in the case of the ABC-flow dynamo, by some other kind of dynamo that is not due to the $\alpha$ effect. While there will always remain some uncertainty regarding the application to the much more extreme astrophysical parameter regime, we can now rule out the possibility of surprising effects within certain limits of $\mathrm{Re_M}$ below 600 and scale separation ratios below 80.

In stars and galaxies, the scale separation ratio is difficult to estimate, but it is hardly above the largest value considered here. This ratio is largest in the top layers of the solar convection zone where the correlation length of the turbulence is short ($1\,\mathrm{Mm}$) compared with the spatial extent of the system ($100\,\mathrm{Mm}$).

Of course, the magnetic Reynolds numbers in the Sun and in galaxies are much larger than what will ever be possible to simulate. Nevertheless, the results presented here show very little dependence of the critical value of $C_\alpha$ on $\mathrm{Re_M}$. For $\mathrm{Pr_M}=1$, for example, we find $C_\alpha^{\rm crit}=1.2$ for $\mathrm{Re_M}\approx 6$ and $C_\alpha^{\rm crit}=1.5$ for $\mathrm{Re_M}\approx 600$. On the other hand, for larger values of $\mathrm{Pr_M}$, the value of $C_\alpha^{\rm crit}$ can drop below unity ($C_\alpha^{\rm crit}=0.9$ for $\mathrm{Pr_M}=100$). While these changes of $C_\alpha^{\rm crit}$ are theoretically not yet understood, it seems clear that they are small and do not provide support for an entirely different scaling law, as anticipated in recent work [11].

### Acknowledgments

The difference between ABC-flows and random plane wave-driven flows was noted during the Nordita Code Comparison Workshop in August 2012, organized by CK Chan, whom we thank for his efforts. We also thank Eric Blackman and Pablo Mininni for useful discussions. This work was supported in part by the European Research Council under the AstroDyn Research Project 227952 and the Swedish Research Council grant 621-2007-4064. Computing resources have been provided by the Swedish National Allocations Committee at the Center for Parallel Computers at the Royal Institute of Technology in Stockholm and Iceland, as well as by the Carnegie Mellon University Supercomputer Center.

[1] E. N. Parker. *Cosmical magnetic fields: Their origin and their activity*. 1979.
[2] H. K. Moffatt. *Magnetic field generation in electrically conducting fluids*. Camb. Univ. Press, 1978.
[3] F. Krause and K.-H. Raedler. *Mean-field magnetohydrodynamics and dynamo theory*. 1980.
[4] N. Seehafer. Nature of the $\alpha$ effect in magnetohydrodynamics. *Phys. Rev. E* , 53:1283–1286, January 1996.
[5] H. Ji. Turbulent dynamos and magnetic helicity. *Phys. Rev. Lett.*, 83:3198–3201, October 1999.
[6] U. Frisch, A. Pouquet, and A. Leorat, J. andMazure. Possibility of an inverse cascade of magnetic helicity in magnetohydrodynamic turbulence. *J. Fluid Mech.*, 68:769–778, 1975.
[7] E. G. Blackman and G. B. Field. Constraints on the magnitude of $\alpha$ in dynamo theory. *ApJ*, 534:984–988, 2000.
[8] E. G. Blackman and G. B. Field. Coronal activity from dynamos in astrophysical rotators. *Mon Not Roy Astron Soc*, 318:724–732, 2000.
[9] N. Kleeorin, D. Moss, I. Rogachevskii, and D. Sokoloff. Helicity balance and steady-state strength of the dynamo generated galactic magnetic field. *Astron. Astrophys.*, 361:L5–L8, September 2000.
[10] A. Brandenburg, S. Candelaresi, and P. Chatterjee. Small-scale magnetic helicity losses from a mean-field dynamo. *Mon Not Roy Astron Soc*, 398:1414–1422, 2009.
[11] J. Pietarila Graham, E. G. Blackman, P. D. Mininni, and A. Pouquet. Not much helicity is needed to drive large-scale dynamos. *Phys. Rev. E* , 85(6):066406, June 2012.
[12] A. Brandenburg. Large-scale dynamos at low magnetic Prandtl numbers. *Astrophys. J.*, 697:1206–1213, June 2009.
[13] A. A. Schekochihin, S. C. Cowley, S. F. Taylor, J. L. Maron, and J. C. McWilliams. Simulations of the small-scale turbulent dynamo. *Astrophys. J.*, 612:276–307, September 2004.
[14] N. E. L. Haugen, A. Brandenburg, and W. Dobler. Simulations of nonhelical hydromagnetic turbulence. *Phys. Rev. E* , 70(1):016308, July 2004.
[15] A. Brandenburg. The Inverse Cascade and Nonlinear Alpha-Effect in Simulations of Isotropic Helical Hydromagnetic Turbulence. *ApJ*, 550:824–840, 2001.
[16] E. G. Blackman and A. Brandenburg. Dynamic nonlinearity in large-scale dynamos with shear. *Astrophys. J.*, 579:359–373, November 2002.
[17] P. J. Käpylä and A. Brandenburg. Turbulent dynamos with shear and fractional helicity. *Astrophys. J.*, 699:1059–1066, July 2009.
[18] B. Galanti, P. L. Sulem, and A. Pouquet. Linear and non-linear dynamos associated with ABC flows. *Geophysical and Astrophysical Fluid Dynamics*, 66:183–208, 1992.
[19] N. Kleeorin, I. Rogachevskii, D. Sokoloff, and D. Tomin. Mean-field dynamos in random Arnold-Beltrami-Childress and Roberts flows. *Phys. Rev. E* , 79(4):046302, 2009.
[20] A. Pouquet, U. Frisch, and J. Leorat. Strong MHD helical turbulence and the nonlinear dynamo effect. *J. Fluid Mech.*, 77:321–354, September 1976.
[21] S. Sur, A. Brandenburg, and K. Subramanian. Kinematic $\alpha$-effect in isotropic turbulence simulations. *Month. Not. Roy. Astron. Soc.*, 385:L15–L19, March 2008.
[22] G. K. Batchelor. *The Theory of Homogeneous Turbulence*.

1953.

[23] P. D. Ditlevsen and P. Giuliani. Cascades in helical turbulence. *Phys. Rev. E* , 63(3):036304, March 2001.

[24] A. Brandenburg. Dissipation in dynamos at low and high magnetic Prandtl numbers. *Astron. Nachr.*, 332:51, January 2011.

[25] A. Hubbard and A. Brandenburg. Catastrophic Quenching in $\alpha\Omega$ Dynamos Revisited. *Astrophys. J.*, 748:51, March 2012.

[26] M. Schrinner, K.-H. Rädler, D. Schmitt, M. Rheinhardt, and U. R. Christensen. Mean-field concept and direct numerical simulations of rotating magnetoconvection and the geodynamo. *Geophysical and Astrophysical Fluid Dynamics*, 101:81–116, 2007.

[27] A. Brandenburg, K.-H. Rädler, and M. Schrinner. Scale dependence of alpha effect and turbulent diffusivity. *Astron. Astrophys.*, 482:739–746, 2008.

[28] K.-H. Rädler and A. Brandenburg. Mean-field effects in the Galloway-Proctor flow. *Month. Not. Roy. Astron. Soc.*, 393:113–125, 2009.

[29] G. B. Field and E. G. Blackman. Dynamical quenching of the $\alpha^2$ dynamo. *Astrophys. J.*, 572:685–692, June 2002.

[30] K. Subramanian. Magnetic helicity in galactic dynamos. *Bull. Astron. Soc. India*, 30:715–721, 2002.